UC Davis

Title

The effect of radiation dose on the onset and progression of radiation-induced brain necrosis in the rat model

Permalink

Journal

ISSN

Authors

Hartl, Brad A
W., Htet S
Hansen, Katherine S
et al.

Publication Date

DOI

The Effect of Radiation Dose on the Onset and Progression of Radiation-Induced Brain Necrosis in the Rat Model

Brad A. Hartl[1], **Htet S. W. Ma**[1], **Katherine S. Hansen**[2], **Julian Perks**[3], **Michael S. Kent**[2], **Ruben C. Fragoso**[3], and **Laura Marcu**[1]

[1]Department of Biomedical Engineering, University of California Davis, USA

[2]Department of Surgical and Radiological Sciences, University of California Davis School of Veterinary Medicine, USA

[3]Department of Radiation Oncology, University of California Davis School of Medicine, USA

Abstract

Purpose—To provide a comprehensive understanding of how the selection of radiation dose affects the temporal and spatial progression of radiation-induced necrosis in the rat model.

Materials and methods—Necrosis was induced with a single fraction of radiation exposure, at doses ranging between 20 and 60 Gy, to the right hemisphere of eight-week-old Fischer rats from a linear accelerator. The development and progression of necrosis in the rats was monitored and quantified every other week with T1- and T2-weighted gadolinium contrast enhanced MRI studies.

Results—The time to onset of necrosis was found to be dose-dependent, but after the initial onset, the necrosis progression rate and total volume generated was constant across different doses ranging between 30 and 60 Gy. Radiation doses less than 30 Gy did not develop necrosis within 33 weeks after treatment, indicating a dose threshold existing between 20 and 30 Gy.

Conclusion—The highest dose used in this study led to the shortest time to onset of radiation-induced necrosis, while producing comparable disease progression dynamics after the onset. Therefore, for the radiation-induced necrosis rat model using a linear accelerator, the most optimum results were generated from a dose of 60 Gy.

Keywords

radiation; necrosis; brain; animal model

Introduction

Clinical management of primary brain tumors, such as glioblastoma, typically consists of a combination of surgical resection, chemotherapy, and fractionated radiotherapy (Stupp et al. 2005). Metastatic tumors to the brain are primarily managed with either whole brain radiation or radiosurgery or a combination of both. Radiotherapy treatments, however, can

have the undesirable effect of generating radiation-induced necrosis in the months to years following treatment, particularly after radiosurgery. The cause of occurrence is not well understood but appears to be dose (Shaw et al. 2002) and fraction size (Ruben et al. 2006) dependent. When combined with chemotherapy there may be up to a five-fold increase in the incidence of radiation-induced necrosis when compared to radiation alone (Ruben et al. 2006). The exact mechanism of radiation-induced brain necrosis is also not well understood (Greene-Schloesser et al. 2012, Siu et al. 2012). One hypothesis is that primary vascular damage results in secondary white matter necrosis due to ischemia. Another proposed mechanism is the parenchymal hypothesis, which involves reaction of either oligodendrocytes, astrocytes, or microglia to radiation damage. The actual mechanism is mostly likely some combination and interaction of all of these effects and thus requires further study and investigation (Greene-Schloesser et al. 2012).

Studying radiation-induced necrosis in patients presents a significant challenge due to the variable incidence rate and time to progression. Small animal models of radiation-induced necrosis, however, represent a useful means to study this treatment related complication. Although it has been established that the radiation-induced necrosis in small animals is representative of the histological features observed in patients (Jiang et al. 2014a, Jiang et al. 2014b, Jiang et al. 2015, Jost et al. 2009, Perez-Torres et al. 2014, Perez-Torres et al. 2015), a limited amount of information exists on the temporal and spatial disease progression. Using stereotactic radiotherapy in mice, the time course of necrotic volumes have been measured with MRI for nine weeks after the onset of necrosis for 60-, 50-, and 45-Gy treatments (Jiang et al. 2015). Although no differences were observed when the radiation dose was fractionated, the authors did find that higher doses correlated to earlier onset of necrosis, matching clinical observations. For studying rats irradiated with a linear accelerator (LINAC), only a limited number of studies have been reported for which the necrosis was assessed at only a single time point (Kumar et al. 2012, Wang et al. 2012a, Wang et al. 2012b, Zhou et al. 2011). For all of these studies, however, there is very limited empirical justification for the radiation doses used or the time-point after radiotherapy treatment when the animals were studied.

The overall objectives of this work are to: (1) assess the effect of radiation dose between 20 and 60 Gy, at 10 Gy intervals, on the temporal characteristics of radiation-induced necrosis in a rat model; specifically evaluating time to onset, rate of progression, and peak volume of necrosis, and (2) assess the anatomic progression of the radiation-induced necrosis through the different structures of the rat brain. The results from this study give critical insight into how the size of the radiation dose affects the spatiotemporal dynamics of necrosis progression in the small animal model, providing for an improved understanding, and ultimately a more accurate model, of brain radiation necrosis.

Materials and methods

Animals

Eight-week-old male Fischer CDF rats (Charles River Laboratories, Wilmington, MA) were used for this study. Rats were used because they are a common model for radiation-induced brain necrosis and also provide a larger volume of tissue to be interrogated relative to mice.

All animal procedures described herein were approved by the Institutional Animal Care and Use Committee of the University of California, Davis (protocol number 18317).

Radiotherapy dose planning and validation

For the purposes of improved dose planning, a set of three animals were imaged on a dedicated computed tomography (CT) scanner (GE Medical Systems, Milwaukee, WI) to provide better anatomic resolution over the cone beam CT incorporated into the LINAC (TrueBeam, Varian Medical Systems, Inc., Palo Alto, CA). Using these images, dose planning and calculation was performed with Eclipse software (Varian Medical Systems, Inc., Palo Alto, CA). This dose plan, as shown in Figure 1, was then co-registered using anatomical landmarks to the LINAC cone-beam pre-exposure images for each of the animals. In order to irradiate a single hemisphere of the brain with minimal dose to the contralateral hemisphere, a square 10×10 mm^2 field was generated with a multileaf collimator, and the rats were treated at a shortened source-to-surface distance of 70 cm to further reduce the field size delivered. A 1-cm-thick bolus was placed on top of the rat's head during treatment to ensure that radiation dose build-up occurred prior to the beam entering the brain parenchyma. Care was taken in selecting the bolus thickness and anatomic location in the skull to minimize the volume of bone and skin tissues receiving full dose, which could potentially lead to necrosis outside of the brain parenchyma. To validate the dose delivered at these small field sizes, a $2 \times 2 \times 1$ mm^3 thermoluminescent dosimeter (Thermo Fisher Scientific, Waltham, MA) was placed inside a 3D-printed photopolymer (MED610, Stratasys Ltd., Eden Prairie, MN) rat phantom. The phantom was then treated with a small dose (~1 Gy) and compared to the treatment plan to generate a correction factor. The field size remained constant for all of the varying treatment doses.

Irradiation

Rats were irradiated with a single fraction of radiation to the right hemisphere using 6 MV photons at a dose rate of 600 MU/min from the LINAC as planned above. Animals were placed in the positioning device used during the imaging procedure, a cone beam CT scan was generated, and the couch was shifted to allow the planned radiation plan to be accurately delivered. Animals received a dose of 20, 30, 40, 50, or 60 Gy (n = 3 per group, except for 60 Gy where n = 6). Animals were anesthetized with isoflurane (2-3%) delivered with a gas anesthesia mask during the treatment and were held in place using a custom-built plastic stereotactic frame.

MR imaging

Progression and development of necrosis in the rats was noninvasively monitored with repeated MRI scans. For these scans T1-weighted images (TR = 1410 ms, TE = 7.5 ms, 0.5 mm slice thickness, 0.5 mm slice spacing, 44 slices total, 3×2 cm^2 field of view, 125×125 μm^2 pixel resolution) as well as T2-weighted images (TR = 6100 ms, TE = 60 ms, 0.5 mm slice thickness, 0.5 mm slice spacing, 44 slices total, 3×2 cm^2 field of view, 125×125 μm^2 pixel resolution) were acquired on a 7 Tesla BioSpec 70/30USR (Bruker Corporation, Billerica, MA). This system was equipped with a 72 mm inner-diameter linear volume coil for transmission and a quadrature surface coil (anatomically shaped for rat brains) for receiving. All animals were injected intraperitoneally with 500 μL of gadodiamide

(Omniscan, GE Healthcare, Chicago, IL), a contrast agent. Isoflurane (2-3%) by inhalation was used to anesthetize the animals during the imaging and a warm air blower was used to maintain body temperature. An initial small group of two animals were scanned every other week to determine the approximate time-point at which pathological necrosis began in the highest treated doses. After establishing this time-point, animals received MRI scans every other week beginning at 15 weeks post radiation exposure. Following the last MRI scan, animals were euthanized and transcardially perfused with saline and then 10% formalin. Tissue slices from the extracted brains were embedded in paraffin, cut and mounted on microscope slides, and were stained with hematoxylin and eosin (H&E). Animals that received a 20- to 50-Gy dose were imaged for 10 weeks; those that received a 60-Gy dose, which was found to be the most relevant for future studies, were imaged for 18 weeks.

Data analysis

The necrotic volume was calculated using a pixel-intensity-comparison method previously described (Jiang et al. 2014a), which primarily measures edema and breakdown of the blood-brain-barrier. This method involved taking the ratio of intensities of a single pixel on the exposed hemisphere to the average of a 5×5 pixel matrix on the contralateral side centered in the same anatomic location. Pixels above a previously determined threshold of 1.4 (based on the upper limit of ratios observed for untreated healthy animals) were denoted as necrosis (Jiang et al. 2014a). Although this method ultimately relies on measurements of the extent of breakdown of the blood-brain-barrier as a proxy for necrosis, it has been shown to agree well with histological grading of necrosis (Jiang et al. 2015).

Results

Temporal disease onset and progression

The volumetric progression of radiation-induced necrosis generated from varying doses are shown quantitatively as volumes versus time in Figure 2a and qualitatively as a time-series progression of MRI images from a single 60-Gy-treated animal in Figure 3. From the volume curves of Figure 2a the onset of necrosis was inversely related to dose, with the highest dose of 60 Gy developing necrosis at the earlier time points. However, MRI- or histology-based evidence of radiation-induced necrosis was not observed at any time-point for any animals receiving less than 30 Gy (Figures 2a and 4a). The volumetric progression rate of radiation-induced necrosis was observed to be independent of total dose (Figure 2a), with the average weekly increase in necrotic volume for the first 8 weeks following the onset of necrosis being approximately 17, 20, 17, and 21 mm³/week for the 30, 40, 50, and 60 Gy exposures, respectively. Correspondingly, the maximum necrotic volume generated for each of these three doses (Figure 2a), was also independent of dose. The brain dose-volume histograms generated from each of the five different treatments plans are plotted in Figure 2b and show the volume of the brain that received at least a certain dose.

Spatial disease progression

At the onset of formation, the necrosis appeared to form along the targeted 100% isodose column (Figure 1a) lateral to the hippocampal formation and thalamus in the corticofugal pathways and striatum (Figure 3). As the necrosis progressed in time—expanding into the

corpus callosum, neocortex, hippocampal formation, and thalamus—it did not appear to be significantly inhibited by any of these structures. However, the most superficial regions of the neocortex never developed necrosis in any treated animal. Due to the rapid progression of the necrosis after the initial onset, as well as the limited time-points where MRI were acquired, the exact focal points of necrosis generation could not be definitively assessed.

The information provided by the T1-weighted and T2-weighted images was not significantly different during the progression of necrosis. Both scan types generated comparable necrotic volumes, contrast uptake, and timing of the initial onset of necrosis. For the purposes of the automated volume quantitation, it was found that the T1-weighted images provided slightly less noisy data. The two image types did, however, provide disparate information at the later stages of the disease where the necrotic volume began to decrease when calculated with the T1-weighted images; these images more directly assess the breakdown of the blood-brain-barrier.

The results of the H&E histology (see Figure 4b and 4e) acquired from the animals at the end of their series of MRI scans showed that the regions of necrosis—as classified using the automated pixel intensity method previously described—contained extensive tissue loss, edema, and fibrinoid vascular necrosis. Micro- hemorrhages and telangiectatic vessels were occasionally, but not consistently, observed in this region. These findings were consistent across all animals that received at least 30 Gy and developed necrosis, independent of radiation dose. Due to the limited time-points at which histology could be acquired for this study and the ability to accurately coregister the two image-sets, a more thorough quantitative comparison between the two was ultimately beyond the intended scope of this paper.

Additional side effects from radiation exposure

The rats tolerated irradiation well with the only major signs being 3-5 mm diameter regions of alopecia that occurred on the tops and bottoms of the head for the 40- through 60-Gy animals. Slight wet desquamation was observed in a few of the 60-Gy animals, but this side effect only persisted for 1-2 weeks and resolved without additional treatment. Weight loss in the animals was minimal, and rarely surpassed 10% of bodyweight. The only neurological deficit observed was that the exposed animals stopped opening up their weekly provided bedding packets at the onset of necrosis development; however, this behaviour only persisted for approximately four weeks. Minor changes in the skull anatomy were present on the treated side of the animal; in addition to slightly thinner bone above the exposed region of the brain, there was a near absence of the temporal line on the right parietal bone (see T1-weighted images of Figure 3). This latter finding, however, did not appear to affect the temporalis muscle attachment or function, as confirmed with necropsy.

Discussion

Temporal disease onset and progression

As observed in the volumetric plots of Figure 2a, the initial onset of radiation-induced necrosis in the tissue was found to be dose dependent, while the progression rate of necrosis

volume was roughly constant across all doses. These trends are in good agreement with previous small animal studies where mice treated with stereotactic radiotherapy over radiation doses between 45 and 60 Gy also found that onset of necrosis, as determined with MRI, was dose-dependent (Jiang et al. 2015). Similar trends have also been observed in humans (Shaw et al. 2002), thus providing further evidence that this animal model is representative of the necrosis process in patients.

A radiation dose threshold appears to exist for generating necrosis, as the animals which received the lowest dose of 20 Gy did not develop any detectible form of necrosis. Given that no necrosis was observed in any of the 20-Gy animals for up to 10 weeks after the initial onset of necrosis in the 30-Gy-exposed animals (Figure 4a), it is unknown if they would have proceeded to develop necrosis in a time frame that is reasonable for experimental studies. Because all of the 30-Gy-exposed animals developed necrosis, this suggests a possible biological threshold above which the risks for radiation necrosis are greater and that the threshold may be between 20 and 30 Gy in this rat model. Although such a threshold has never been observed in rodents using a LINAC and monitoring with MRI, necrosis formation was not observed histologically in animals that were treated with stereotactic radiotherapy receiving 30-, 40-, 50-, or 60-Gy peak doses (Kondziolka et al. 1992). While this is somewhat contradictory to the observations of the present study, it is important to note that the previous study only followed the animals for just under 13 weeks. Had the animals been followed for a few more weeks, necrosis may have been observed in some of the animals.

Translating a radiation dose threshold between 20 and 30 Gy to the dose-volume histogram (Figure 2b), one would have expected larger peak-necrotic volumes in Figure 2a. For the 60-Gy treatment as an example, applying such a threshold would suggest that the necrotic volume should lie between 285 and 330 mm^3, significantly higher than the volumes generated. A dose threshold of 20 to 30 Gy would also suggest that the 60-Gy treatment should have produced up to 38% more necrosis than the 30-Gy treatment, which contradicts the relatively constant total volume generated across the different doses. These disparities, however, can potentially be explained by the susceptibility of necrosis development in certain anatomic regions of the brain (notably the neocortex, as discussed in the proceeding section). Thus, the additional volume that received doses above the threshold could have been located in regions where the tissue was less susceptible to necrosis progression.

This volumetric analysis of the necrosis progression demonstrates that a 60-Gy exposure is a superior dose compared to all lower doses for rat models of radiation-induced necrosis using a LINAC. By generating the necrosis earlier, it significantly reduces the time to study radiation-induced necrosis, while producing comparably representative necrotic tissue. The 60-Gy treatment also generated necrosis approximately five weeks earlier than the more commonly used 40-Gy dose, while not inducing any additional adverse effects. This may also be more humane for the animals and there is less cost associated with the study.

Spatial disease progression

Despite it falling well within the region receiving the targeted 100% dose, the most superficial regions of the neocortex (Figure 3) did not develop necrosis in any of the treated

animals. This effect can potentially be attributed to the more vascularized nature of the neocortex, where the additional blood supply may reduce the ischemia caused by the necrosis. The healing process of the blood-brain-barrier in the 60-Gy-treated animals can readily be observed in both Figures 2a with the decrease in necrotic volume and Figure 3 with the accumulation of fluid-like regions. The H&E histology acquired at the end of the MRI series also confirms this (Figure 4c and 4f), showing widespread clearing of the cellular debris in the regions where necrosis was present. Although from clinical experience, this healing process is to be expected, it has never been directly observed or monitored in rodent models of radiation-induced necrosis before. From the volumetric studies, this reversal of necrotic volume appears to have occurred around 8-10 weeks after the onset of necrosis. After this time period, the progressive healing of the blood-brain-barrier (T1-weighted images of Figure 3) as well as accumulation of fluid (hyperintense regions of T2-weighted images in Figure 3) was observed. These results underscore the fact that when studying radiation-induced necrosis with this model, it is imperative to assess the tissue within eight weeks after the onset of necrosis.

Although investigating the pathomechanisms of radiation-induced necrosis was beyond the intended scope of this work, the histological features observed in the tissue at the end of the imaging studies, such as extensive tissue loss, edema, and fibrinoid vascular necrosis, were in good agreement with those found in previous experiments where H&E histology and MRI images were acquired (Jiang et al. 2015). Although histology was only acquired at a single time-point—approximately peak necrosis volume for each dose—the histological features were not significantly different across the different doses. This finding is in agreement with previous studies, which found that more advanced histological signs of necrosis correlated with volume of necrosis, as opposed to the dose of radiation delivered (Jiang et al. 2015). Given that this previous study was performed in mice with a Gamma Knife radiotherapy unit, in contrast to the rats and LINAC used herein, the agreement of the histological outcomes provides further evidence for the translatability of the spatiotemporal necrosis progression findings from this study to other models of radiation-induced necrosis.

Additional side effects from radiotherapy

The minimal side effects observed from the radiation treatments provide further evidence for the utility of the rat model for studying radiation-induced brain necrosis. Future studies could potentially evaluate the use of LINAC doses higher than 60 Gy to assess whether the onset of necrosis could be generated even earlier in time with similar progression dynamics.

Conclusion

This study evaluated how the size of radiation dose affects the spatial and temporal progression of radiation-induced necrosis in a small animal model. For single-fraction-radiation-treated rats, the time to necrosis onset was found to be dose-dependent, but after the initial onset, the necrosis progression rate and total volume generated was constant across different doses ranging between 30 and 60 Gy. A maximum necrotic volume appeared to occur at approximately 8-10 weeks after the onset of necrosis, with the healing of the blood-brain-barrier progressing after this time point. Importantly, it was also observed

that radiation doses less than 30 Gy never generated necrosis within 33 weeks after treatment, suggests a possible dose threshold between 20 and 30 Gy for the observation period. Correspondingly, the volumes of necrosis generated did not correlate with the volume exposed—assuming a threshold existing between 20-30 Gy—which was attributed to anatomic regions of the brains being more radio-resistant than others, most notably the neocortex. Ultimately, for a single-fraction treatment the highest dose tested of 60 Gy was the most efficient relative to any lower doses for generating radiation-induced brain necrosis. The 60-Gy dose generated necrosis the quickest while following the same spatiotemporal progression of the disease as the other lower doses with no additional adverse effects. The results from this study have contributed useful insight into the development and progression of radiation-induced brain necrosis, as well as providing significant and critical information for the planning and performing of such experiments.

Acknowledgments

References

Greene-Schloesser D, Robbins ME, Peiffer AM, Shaw EG, Wheeler KT, Chan MD. Radiation-induced brain injury: A review. Front Oncol. 2012; 2:73. [PubMed: 22833841]

Jiang XY, Engelbach JA, Yuan LY, Cates J, Gao F, Drzymala RE, Hallahan DE, Rich KM, Schmidt RE, Ackerman JJH, et al. Anti-VEGF Antibodies Mitigate the Development of Radiation Necrosis in Mouse Brain. Clin Cancer Res. 2014a; 20:2695–2702. [PubMed: 24647570]

Jiang XY, Perez-Torres CJ, Thotala D, Engelbach JA, Yuan LY, Cates J, Gao F, Drzymala RE, Rich KM, Schmidt RE, et al. A GSK-3 beta Inhibitor Protects Against Radiation Necrosis in Mouse Brain. Int J Radiat Oncol. 2014b; 89:714–721.

Jiang XY, Yuan LY, Engelbach JA, Cates J, Perez-Torres CJ, Gao F, Thotala D, Drzymala RE, Schmidt RE, Rich KM, et al. A Gamma-Knife-Enabled Mouse Model of Cerebral Single-Hemisphere Delayed Radiation Necrosis. Plos One. 2015; 10

Jost SC, Hope A, Kiehl E, Perry A, Travers S, Garbow JR. A Novel Murine Model for Localized Radiation Necrosis and Its Characterization Using Advanced Magnetic Resonance Imaging. Int J Radiat Oncol. 2009; 75:527–533.

Kondziolka D, Lunsford LD, Claassen D, Maitz AH, Flickinger JC. Radiobiology of radiosurgery:Part I. The normal rat brain model. Neurosurgery. 1992; 31:271–279. [PubMed: 1513433]

Kumar S, Arbab AS, Jain R, Kim J, deCarvalho AC, Shankar A, Mikkelsen T, Brown SL. Development of a novel animal model to differentiate radiation necrosis from tumor recurrence. J Neuro-Oncol. 2012; 108:411–420.

Perez-Torres CJ, Engelbach JA, Cates J, Thotala D, Yuan L, Schmidt RE, Rich KM, Drzymala RE, Ackerman JJ, Garbow JR. Toward distinguishing recurrent tumor from radiation necrosis: DWI and MTC in a Gamma Knife--irradiated mouse glioma model. Int J Radiat Oncol Biol Phys. 2014; 90:446–453. [PubMed: 25104071]

Perez-Torres CJ, Yuan LY, Schmidt RE, Rich KM, Ackerman JJH, Garbow JR. Perilesional edema in radiation necrosis reflects axonal degeneration. Radiat Oncol. 2015; 10

Ruben JD, Dally M, Bailey M, Smith R, McLean CA, Fedele P. Cerebral radiation necrosis: incidence, outcomes, and risk factors with emphasis on radiation parameters and chemotherapy. Int J Radiat Oncol Biol Phys. 2006; 65:499–508. [PubMed: 16517093]

Shaw E, Arusell R, Scheithauer B, O'Fallon J, O'Neill B, Dinapoli R, Nelson D, Earle J, Jones C, Cascino T, et al. Prospective randomized trial of low- versus high-dose radiation therapy in adults with supratentorial low-grade glioma: initial report of a North Central Cancer Treatment Group/ Radiation Therapy Oncology Group/Eastern Cooperative Oncology Group study. J Clin Oncol. 2002; 20:2267–2276. [PubMed: 11980997]

Siu A, Wind JJ, Iorgulescu JB, Chan TA, Yamada Y, Sherman JH. Radiation necrosis following treatment of high grade glioma--a review of the literature and current understanding. Acta Neurochir (Wien). 2012; 154:191–201. discussion 201. [PubMed: 22130634]

Stupp R, Mason WP, van den Bent MJ, Weller M, Fisher B, Taphoorn MJ, Belanger K, Brandes AA, Marosi C, Bogdahn U, et al. Radiotherapy plus concomitant and adjuvant temozolomide for glioblastoma. N Engl J Med. 2005; 352:987–996. [PubMed: 15758009]

Wang SL, Chen YF, Lal B, Ford E, Tryggestad E, Armour M, Yan K, Laterra J, Zhou JY. Evaluation of radiation necrosis and malignant glioma in rat models using diffusion tensor MR imaging. J Neuro-Oncol. 2012a; 107:51–60.

Wang SL, Tryggestad E, Zhou TT, Armour M, Wen ZB, Fu DX, Ford E, van Zijl PCM, Zhou JY. Assessment of MRI Parameters as Imaging Biomarkers for Radiation Necrosis in the Rat Brain. Int J Radiat Oncol. 2012b; 83:E431–E436.

Zhou JY, Tryggestad E, Wen ZB, Lal B, Zhou TT, Grossman R, Wang SL, Yan K, Fu DX, Ford E, et al. Differentiation between glioma and radiation necrosis using molecular magnetic resonance imaging of endogenous proteins and peptides. Nat Med. 2011; 17:130–U308. [PubMed: 21170048]
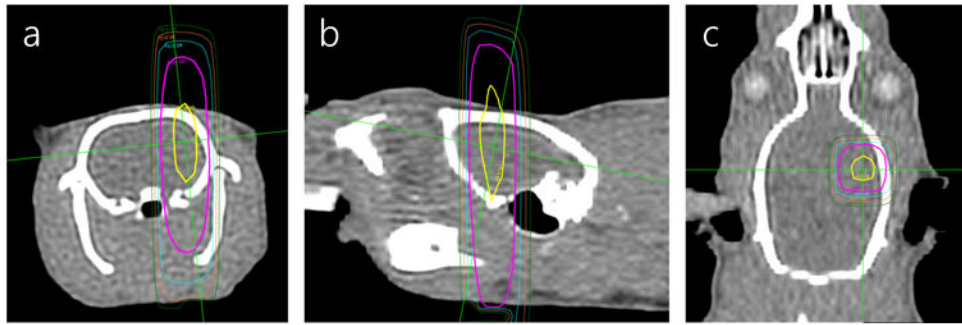
Figure 1.
Radiation dose plan overlaid onto computed tomography images of a rat showing coronal, sagittal, and transverse axis (a-c, respectively). Relative isodose lines are shown for the range 100% (yellow), 83% (magenta), 67% (teal), 50% (orange), and 33% (dark green). The 1-cm bolus placed on top of the animal during irradiation is not shown here. Crosshair lines (green) indicate the locations of the orthogonal imaging planes.
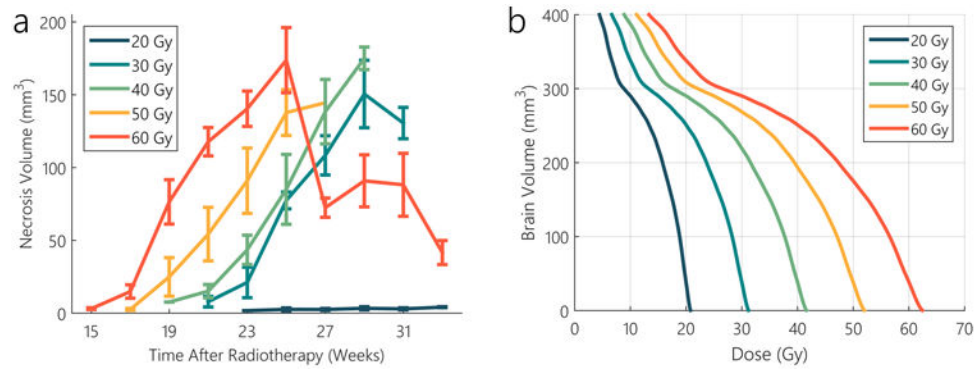
Figure 2.
MRI-derived necrosis volumes over time after treatment with varying single fraction radiation doses, S.E.M. are included for the different treatment groups (a); treatment planning dose-volume histograms for each of the corresponding doses (b).
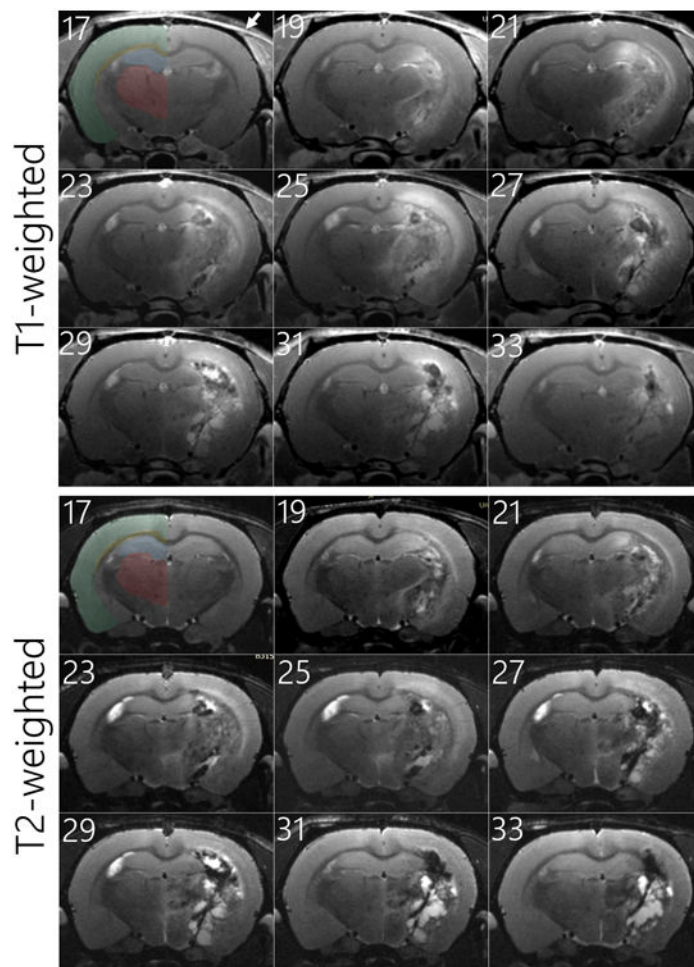
Figure 3.
The progression of necrosis (hyperintense region in the right hemisphere) from a single animal as tracked with MRI from 17 through 33 weeks after a single fraction 60-Gy radiotherapy treatment (with weeks labelled in upper left corner of each image). The gadolinium contrast-enhanced T1-weighted (top) and T2-weighted (bottom) MRI image slices were selected at the craniocaudal center of radiation-induced necrosis development. Major anatomic regions have been shaded for the untreated left hemisphere of the first image; neocortex (green), corpus callosum (yellow), hippocampal formation (blue), and thalamus (red). The absence of the temporal line on the right parietal bone has been denoted with a white arrow.
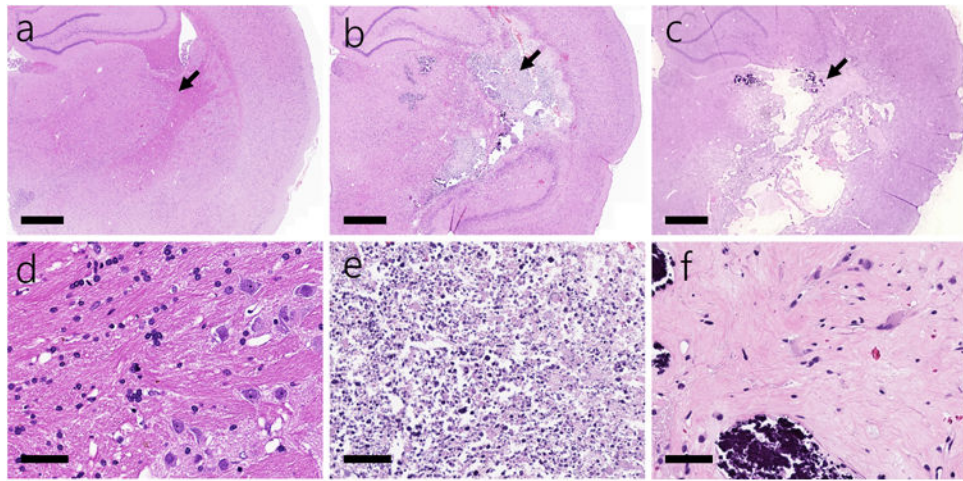
Figure 4.
Representative coronal sliced H&E stained histology from the irradiated, right hemispheres of the 20-Gy animals—which did not form necrosis in the duration of the study (a), 30-through 60-Gy animals at approximate peak necrosis volume (b), and 60-Gy animals at terminus of study (c); black arrows indicate the location of corresponding zoomed in images below for each of the three cases (d-f). Scale bars are 1.0 mm (top images) and 50 μm (bottom images).